

## Dependence of multiplicity and rapidity distributions on the number of projectile collisions in 200-GeV/c proton-nucleus interactions

C. De Marzo, M. De Palma, A. Distanto, C. Favuzzi, P. Lavopa, G. Maggi, F. Posa, A. Ranieri, G. Selvaggi, P. Spinelli, and F. Waldner

*Dipartimento di Fisica dell'Università di Bari and Istituto Nazionale de Fisica Nucleare, Bari, Italy*

T. Coghen, J. Chwastowski, A. Eskreys, K. Eskreys, D. Kisielewska, A. Kotarba, P. Malecki, A. B. Michalowska, K. Olkiewicz, B. Pawlik, and P. Stopa

*Institute of Nuclear Physics, Institute of Physics and Nuclear Techniques of Academy of Mining and Metallurgy, Krakow, Poland*

J. R. Fry, C. Grant, M. A. Houlden, and S. L. Wong

*University of Liverpool, Liverpool, United Kingdom*

F. Dengler, I. Derado, V. Eckardt, J. Fent, P. Freund, H. J. Gebauer, A. Manz, P. Polakos,

K. P. Pretzl, N. Schmitz, T. Schouten, P. Seyboth, J. Seyerlein, D. Vranic, and G. Wolf

*Max-Planck-Institut für Physik und Astrophysik, München, Federal Republic of Germany*

F. Crijns, W. J. Metzger, C. Pols, and T. Spuijbroek

*University of Nijmegen and NIKHEF, Nijmegen, Netherlands*

(Received 28 November 1983)

Interactions of 200-GeV/c protons on hydrogen, neon, argon, and xenon were studied with a streamer-chamber spectrometer. The number of projectile collisions inside the nucleus and the number of secondary collisions in the intranuclear cascade were estimated. The dependence of multiplicity and rapidity distributions on the number of projectile collisions was analyzed. The predictions of the additive quark model were found to be in qualitative agreement with the results of the experiment.

### I. INTRODUCTION

Most models describing interactions of hadrons with nuclei are based on the hypothesis of multiple collisions of a projectile inside the target nucleus. In these models the production of particles occurs in the process of the independent collisions of a beam particle or its constituents with the nucleons of the target nucleus.<sup>1,2</sup> One of the simplest of this type of model is the additive quark model (AQM).<sup>2</sup> In this model the interactions take place between the valence quarks of the projectile and the nucleons inside the nucleus. Each quark may pass through the nucleus without any collision or may collide once or several times independently of what happens to the other valence quarks. In any particular event a definite number of collisions  $\nu$  occurs. This  $\nu$  is the basic, natural parameter of the model, the knowledge of which is of great importance for checking the predictions. A very crude estimate of this number is the average

$$\bar{\nu}_A = \frac{A\sigma_{hN}}{\sigma_{hA}} \quad (1)$$

calculated for a given nucleus<sup>3</sup> where  $\sigma_{hN}$  and  $\sigma_{hA}$  are the cross sections for a hadron  $h$  interacting with a nucleon or a nucleus of atomic number  $A$ , respectively. This  $\bar{\nu}$ , however, is an average of  $\nu$  over a presumably very broad

probability distribution  $\pi_A(\nu)$ . A better determination of the number  $\nu$  of projectile collisions is very desirable. In the present analysis we have made an attempt to extract this number from the data on proton interactions with hydrogen, neon, argon, and xenon nuclei at 200 GeV/c.

The data were collected in the NA5 experiment at the CERN SPS using a streamer-chamber spectrometer. Our present study is based on a sample of 5900 nuclear interactions with three or more charged particles in the final state which separate into reactions on four nuclear targets as shown in Table I. The details of the experimental configuration and the reconstruction procedure can be found in our earlier publication.<sup>4</sup>

In our experiment there was no identification of particles beyond that based on the ionization and the charge of tracks observed in the streamer chamber. Thus we could identify slow protons, i.e., of momenta below 600 MeV/c. All other tracks were treated as pions and are referred to as produced particles in the following. The use of track-insensitive targets in our experiment (Mylar tubes filled with liquid H<sub>2</sub> or Ar or Xe gas) limits the momenta of visible protons to be greater than about 100 MeV/c. Thus in the momentum interval 100 to 600 MeV/c we have rather good identification of knocked out protons. Heavy nuclear fragments have little chance of leaving the gas target in our experimental setup.

TABLE I. Number of events used in the analysis.

Reaction	Number of events with three or more charged particles
$pp$	3340
$p\text{Ne}$	270
$p\text{Ar}$	929
$p\text{Xe}$	1362

## II. ESTIMATION OF THE NUMBER OF PROJECTILE COLLISIONS INSIDE THE NUCLEUS

Several methods of estimating  $\nu$  have been proposed.<sup>5</sup> Most of them exploit the expected correlation between the number of protons knocked out of the nucleus during the passage of the projectile and the number of projectile collisions. In our analysis we have adopted the method proposed by Andersson, Otterlund, and Stenlund.<sup>5</sup> In this method it is assumed that an incident hadron or its constituents (for simplicity referred to henceforth as "a projectile") on their passage through a nucleus strike the target nucleons, which have a good chance of leaving the nucleus without further interaction. If these struck nucleons are protons they can be observed as highly ionizing, positively charged particles. However, such protons can also be knocked out in the collision of a secondary particle coming from the projectile collision, while it propagates through the nucleus. This process is known in the literature as a "cascade."<sup>6</sup> Thus, in order to relate the number of projectile collisions  $\nu$  to the number of observed protons  $n_p$ , one has to disentangle these two types of processes.

In the model of Andersson *et al.* one assumes that each projectile collision inside a nucleus of a mass number  $A$  leads to an identical probability distribution of knocked out protons  $P_{\nu=1}^A(n_p)$  (the notation is that of Andersson *et al.*<sup>5</sup>). This distribution, however, may depend on the nucleus  $A$ . In the paper by Andersson *et al.* it was parametrized on the basis of the emulsion data<sup>7</sup> as

$$P_{\nu=1}^A(n_p) = (1-x)x^{n_p}, \quad (2)$$

where

$$x = (\langle n_p \rangle_A / \bar{\nu}_A) / (1 + \langle n_p \rangle_A / \bar{\nu}_A)$$

and  $\langle n_p \rangle_A / \bar{\nu}_A$  is the average number of knocked out protons in one collision. One may attempt to determine  $P_{\nu=1}^A(n_p)$  separately for any nucleus  $A$  by analyzing events which result from a single projectile collision. By making suitable cuts on the data one can isolate such a sample of events. The overall probability distribution of  $n_p$  for  $\nu$  projectile collisions in a nucleus  $A$  is a convolution of  $\nu$  independent distributions:

$$P_{\nu}^A(n_p) = \binom{n_p + \nu - 1}{n_p} (1-x)^{\nu} x^{n_p}. \quad (3)$$

Knowing the total inelastic cross sections it is possible to calculate in the Glauber model the probability  $\pi_A(\nu)$  that

the projectile collides  $\nu$  times inside the nucleus of mass  $A$ . Using  $\pi_A(\nu)$  and formulas (2) and (3) one obtains the average number of projectile collisions,  $\bar{\nu}(n_p)$ , for a class of events with a given number  $n_p$  of knocked-out protons

$$\bar{\nu}(n_p) = \sum_{\nu} \nu \pi_A(\nu) P_{\nu}^A(n_p) / \sum_{\nu} \pi_A(\nu) P_{\nu}^A(n_p). \quad (4)$$

The result of this calculation for Xe and Ar nuclei is shown in Fig. 1.

In order to check if the parametrization (2) is also suitable for our data we have attempted to select that sample of events corresponding to single projectile collisions. Such events should have (i) at least one energetic particle, presumably coming from the projectile and (ii) multiplicity below the average since multiple projectile collisions lead to large average multiplicities.

With a cut of multiplicity at 18 for Xe and 15 for Ar and the requirement of at least one particle with rapidity  $y > 5$  for both nuclei we get distributions of the number of visible protons shown by the full circles in Figs. 2(a) and 2(b). These distributions are well reproduced by the parametrization (2) (full curves<sup>8</sup>) and do not depend critically on either cut. The distributions of  $n_p$  for all events  $P(n_p)$  are shown in Figs. 2(a) and 2(b) by open circles. They can also be calculated

$$P(n_p) = \sum_{\nu} \pi_A(\nu) P_{\nu}^A(n_p). \quad (5)$$

The result of this calculation is shown by the dashed curves in Figs. 2(a) and 2(b) and agrees qualitatively with the data. We thus conclude that  $\bar{\nu}(n_p)$  as calculated from formula (4) can be used as an approximation to the real number of projectile collisions.

As shown in Fig. 1, the dependence of  $\bar{\nu}(n_p)$  on  $n_p$  is not linear. For a class of events with a given number  $n_p$  of knocked-out protons,  $\bar{\nu}(n_p)$  according to formula (4) is the average of the number of projectile collisions  $\nu$ , i.e., the first moment of the distribution of the number  $\nu$  of projectile collisions for this class of events. In an analogous way any higher moment of this distribution can be calculated. In particular the dispersion  $\Delta$  is of interest as it measures the broadness of the distribution. The depen-

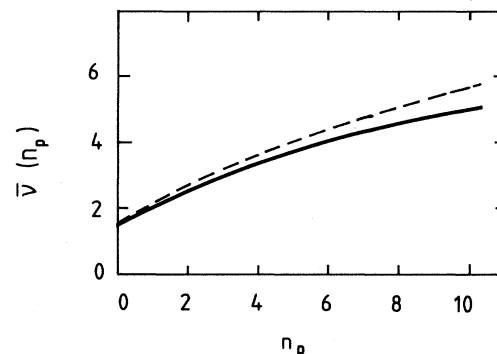


FIG. 1. Average number  $\bar{\nu}(n_p)$  of projectile collisions versus the number  $n_p$  of knocked-out protons calculated from Eq. (4) for  $p\text{Ar}$  ( $x=0.446$ , solid curve) and  $p\text{Xe}$  ( $x=0.541$ , dashed curve) reactions.

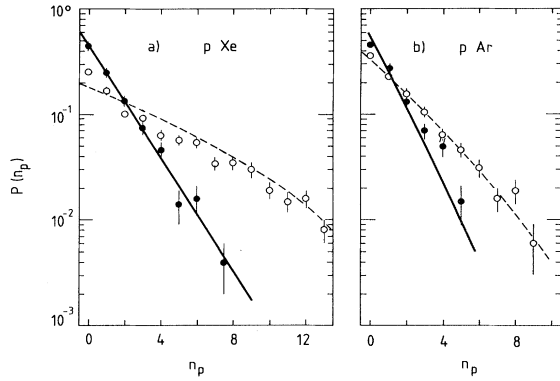


FIG. 2. Probability  $P(n_p)$  for producing  $n_p$  visible protons in (a)  $p$ Xe and (b)  $p$ Ar collisions. The open circles and the full circles show the data for all collisions and for those producing at least one charged particle with rapidity  $y > 5$ , respectively. Solid and dashed curves were calculated from Eqs. (2) and (5), respectively.

dence of  $\Delta$  on  $\bar{\nu}(n_p)$  is shown by the full curve in Fig. 3. It is seen to be smaller than the dispersion for all events (all  $n_p$ , dashed line in Fig. 3), i.e., of the distribution  $\pi_A(\nu)$ . This indicates that  $\bar{\nu}(n_p)$  is a better measure of the number of the projectile collisions than the commonly used quantity  $\bar{\nu}_A$ .

It should be stressed at this point that within the approach described above the data on collisions with nuclei of fixed mass  $A$  supply information on interactions with different numbers of projectile collisions  $\bar{\nu}(n_p)$ . For Xe  $\bar{\nu}(n_p)$  reaches values above 5 (in an experiment with higher statistics this value could be even higher), whereas even for the heaviest nucleus (uranium),  $\bar{\nu}_A$  is only 4 according to Eq. (1). The averages of  $\bar{\nu}(n_p)$  over  $n_p$  ( $2.84 \pm 0.32$  for Xe and  $2.33 \pm 0.26$  for Ar) are close to the value of  $\bar{\nu}_A$  (Ref. 8) as expected.

### III. ANALYSIS OF THE DATA IN TERMS OF THE PARAMETER $\bar{\nu}(n_p)$

#### A. Multiplicity distribution of charged particles

The commonly adopted measure of the overall multiplication of particles in the interaction with a nucleus is the ratio  $R = \langle n \rangle_{hA} / \langle n \rangle_{hp}$  where  $\langle n \rangle_{hA}$  and  $\langle n \rangle_{hp}$  are the average charged multiplicities of produced particles in collisions with a nucleus and a proton, respectively. The dependence of  $R$  on the number of projectile collisions was found to be linear.<sup>9</sup> In the literature one usually plots  $R$  vs  $\bar{\nu}_A$  with the maximum value of  $\bar{\nu}_A = 4$  for uranium. In our analysis we have been able to extend this range by using  $\bar{\nu}(n_p)$  instead of  $\bar{\nu}_A$ . As seen from Fig. 4 the relation between  $R$  and  $\bar{\nu}(n_p)$  remains linear over this extended range of  $\bar{\nu}(n_p)$ . The relation is the same as that found using the variable  $\bar{\nu}_A$ .<sup>9</sup> The linear increase of  $R$  with  $\bar{\nu}(n_p)$  is consistent with the natural expectation that the average charged multiplicity should increase with the number of projectile collisions.

We have also analyzed the dispersion

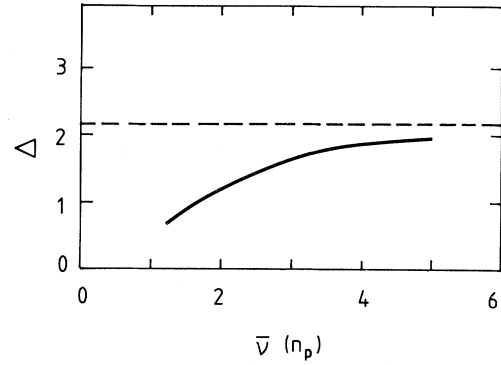


FIG. 3. The dispersion  $\Delta$  of the distribution of the number  $\nu$  of projectile collisions calculated for a class of events with a given number  $n_p$  of knocked-out protons is plotted versus  $\bar{\nu}(n_p)$  (full line). The dashed line shows the value of the dispersion of the distribution of  $\nu$  for all values of  $n_p$ .

$$D = (\langle n^2 \rangle - \langle n \rangle^2)^{1/2}$$

of the multiplicity distribution and  $D/\langle n \rangle$ . Their dependence on  $\bar{\nu}(n_p)$  is shown in Figs. 5 and 6. We observe that  $D/\langle n \rangle$  decreases with  $\bar{\nu}(n_p)$  in the same way for Ar and Xe. In contrast  $D/\langle n \rangle$  of the total multiplicity distribution (all  $n_p$ ) was found to be constant for various nuclei,<sup>4,9</sup> i.e., independent of  $\bar{\nu}_A$ . One can qualitatively understand this effect as an interplay of two mechanisms:<sup>10</sup> (i) the variation of  $D$  and  $\langle n \rangle$  with the number of projectile collisions  $\nu$  like

$$D^2 = a + b\nu \text{ and } \langle n \rangle = c + d\nu, \quad (6)$$

and (ii) an increase of  $D$  due to the fact that events with a different number of projectile collisions  $\nu$  contribute.

#### B. Rapidity distributions

Rapidity

$$y = \frac{1}{2} \ln[(E + p_L)/(E - p_L)]$$

and pseudorapidity

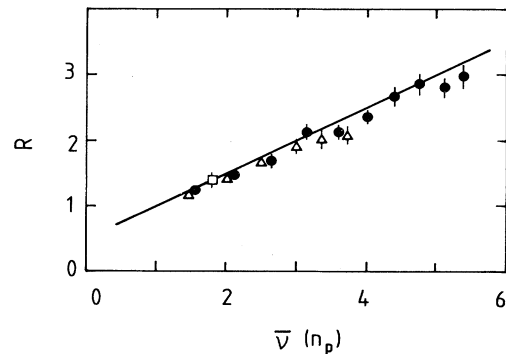


FIG. 4. The ratio  $R = \langle n \rangle_{pA} / \langle n \rangle_{pp}$  versus the average number  $\bar{\nu}(n_p)$  of projectile collisions for  $p$ Xe (circles),  $p$ Ar (triangles), and  $p$ Ne (squares) collisions. A line of the form  $R = 0.5[\bar{\nu}(n_p) + 1]$  is shown for comparison.

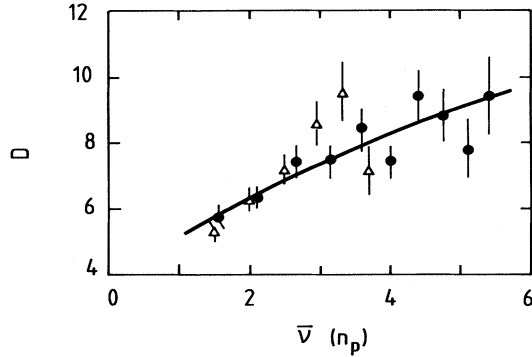


FIG. 5. Dispersion  $D$  of the distribution of the number of produced particles versus  $\bar{v}(n_p)$  for  $p$ Xe (circles) and  $p$ Ar (triangles) collisions. The curve is a fit of the form (6).

$$\eta = \ln \tan \theta / 2$$

have been commonly used as variables in the description of the kinematics of hadron-nucleus collisions. We were able to use rapidity since the momenta of all observed particles were measured and most slow protons were identified. The rapidity interval can be divided into three regions where one believes that different production mechanisms dominate: (i) the target fragmentation region,  $y < 2.0$ ; (ii) the central production region,  $2.4 < y < 3.6$ ; (iii) the beam fragmentation region,  $y > 5.0$ .

This particular choice of rapidity regions was motivated by Fig. 7 in which the multiplication ratio

$$R(y) = (d\sigma/dy)_{pA} / (d\sigma/dy)_{pp}$$

for Ne, Ar, and Xe targets is shown. It should be noted that the rapidity regions were chosen noncontiguous in order to remove the transition regions. In the following analysis we will now discuss the behavior of  $R(y)$  and  $D/\langle n \rangle$  in these three regions as a function of  $\bar{v}(n_p)$ , where  $n$  is now the number of produced particles within each rapidity region.

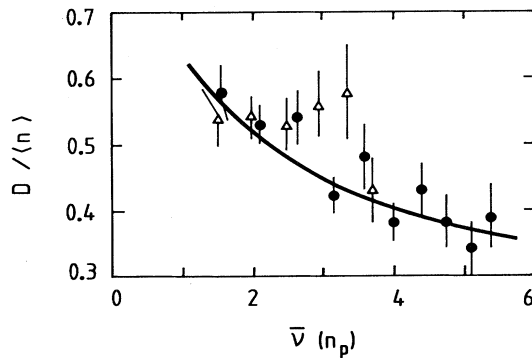


FIG. 6. Ratio  $D/\langle n \rangle$  of the distribution of the number of produced particles versus  $\bar{v}(n_p)$  for  $p$ Xe (circles) and  $p$ Ar (triangles) collisions. The curve is a fit of the form (6).

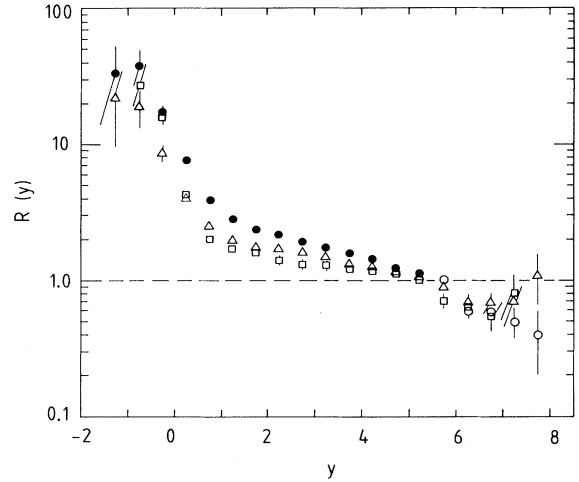


FIG. 7. The particle multiplication ratio  $R(y) = (d\sigma/dy)_{pA} / (d\sigma/dy)_{pp}$  for  $p$ Xe (circles),  $p$ Ar (triangles), and  $p$ Ne (squares) collisions versus the rapidity  $y$ .

### 1. Target-fragmentation region

In this part of phase space the bulk of produced particles comes from a cascade process.<sup>4,6</sup> It is believed that in such a process the particles produced in the primary collision of the projectile, while propagating through the nucleus, can collide and produce the next generation of particles. This happens when the formation zone  $L_f$  of the particle [ $L_f \simeq p/m^2$  (Ref. 11) where  $p$  is the momentum and  $m$  is the mass of the particles] is smaller than its potential path inside the nucleus and smaller than the nuclear radius  $r_A$ . Such a process can be repeated several times depending on the size of the formation zone and the size of the nucleus. Thus fast multiplication of slow particles occurs, since such particles can meet the condition  $L_f < r_A$ . In Figs. 8(a) and 9(a) we show for the target fragmentation region the dependence of  $\tilde{R}$  [the average of  $R(y)$  in this rapidity interval] and  $D/\langle n \rangle$  on  $\bar{v}(n_p)$  for Ne, Ar, and Xe nuclei. We observe the same behavior for all nuclei, i.e.,  $\tilde{R}$  and  $D/\langle n \rangle$  depend only on  $\bar{v}(n_p)$ . The expected increase of  $\tilde{R}$  with  $\bar{v}(n_p)$  is to a good approximation linear, while  $D/\langle n \rangle$  decreases like  $1/[\bar{v}(n_p)]^{1/2}$  [the curve in Fig. 9(a) is a fit of the form (6)]. These results are consistent with the picture of independent multiple collisions of an object inside the nucleus.

### 2. Central production region

In the central production region direct production of particles dominates and contributions from cascading are negligible.<sup>4</sup> Many models predict a plateau of  $R(y)$  in this region, which, for example, in the AQM is proportional to the average number of interacting quarks for a given nucleus. Our measurements in this region are

$$\tilde{R}^{Xe} : \tilde{R}^{Ar} : \tilde{R}^{Ne} = (1.84 \pm 04) : (1.58 \pm 04) : (1.30 \pm 06) .$$

They agree well with the prediction:<sup>12</sup>

$$\tilde{R}^{Xe} : \tilde{R}^{Ar} : \tilde{R}^{Ne} = 1.93 : 1.59 : 1.49 .$$

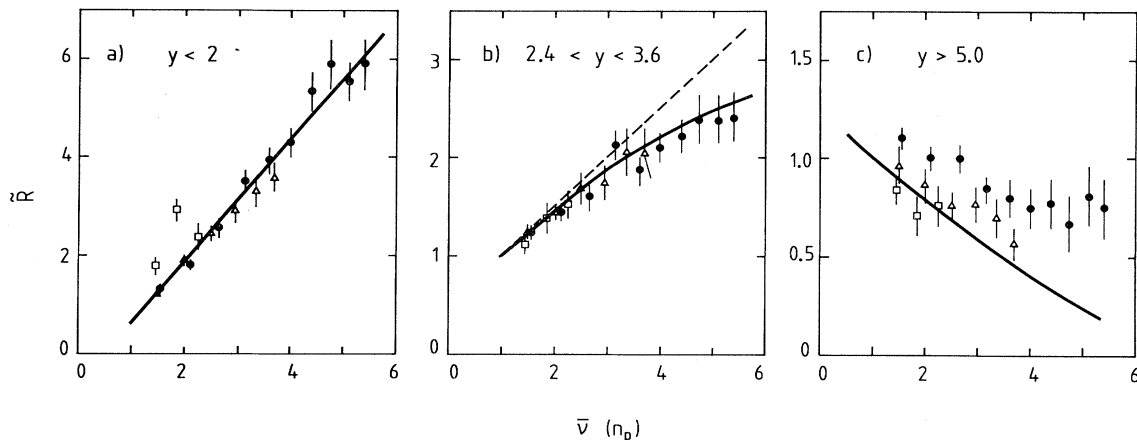


FIG. 8. Average  $\tilde{R}$  of  $R(y)$  in (a) the target fragmentation, (b) the central production, and (c) the beam fragmentation regions versus  $\bar{\nu}(n_p)$ . Data for  $p\text{Xe}$ ,  $p\text{Ar}$ , and  $p\text{Ne}$  reactions are shown by circles, triangles, and squares, respectively. Predictions of the AQM and the dual parton model are shown by the solid and dashed curves, respectively.

Plots of  $\tilde{R}$  and  $D/\langle n \rangle$  vs  $\bar{\nu}(n_p)$  are shown in Figs. 8(b) and 9(b). One observes that  $\tilde{R}$  increases more slowly with  $\bar{\nu}(n_p)$  than in the target fragmentation region. In fact,  $\tilde{R}$  may saturate at large  $\bar{\nu}(n_p)$  at a level of about 3. As seen from Fig. 9(b),  $D/\langle n \rangle$  initially decreases with increasing  $\bar{\nu}(n_p)$  but then also seems to level off. This behavior of both  $\tilde{R}$  and  $D/\langle n \rangle$  for large values of  $\bar{\nu}(n_p)$  could be interpreted as evidence that only a small number of initial collisions of a projectile are “effective” in producing particles in the central region. This number is consistent with 3 expected, e.g., by the AQM.<sup>2</sup> It is interesting to note that the distinction between different models, e.g., the additive quark model (full curves<sup>12</sup> in Figs. 8 and 9) and the dual parton model<sup>13</sup> [dashed curve in Fig. 8(b)] is possible only for a number of projectile collisions greater than 4. For large values of  $\bar{\nu}(n_p)$  the AQM seems to reproduce the data better.

### 3. Beam fragmentation region

In this region our experiment has the largest uncertainties. Produced particles are fast and therefore their momenta are measured less accurately and they cannot be identified. As seen from Fig. 7,  $R(y)$  falls below unity for large  $y$  confirming earlier indications.<sup>14</sup> The dependence of the average  $\tilde{R}$  on  $\bar{\nu}(n_p)$  is shown in Fig. 8(c). It seems that the number of produced particles in the beam fragmentation region decreases with increasing number of collisions  $\bar{\nu}(n_p)$ .

Intuitively one expects that the more collisions occur, the more energy is dissipated for the production of particles. As a consequence any surviving projectile particle and the produced particles are less energetic. The AQM follows the trend of the data also in the beam fragmentation region as seen from the curves in Figs. 8(c) and 9(c).<sup>12</sup>

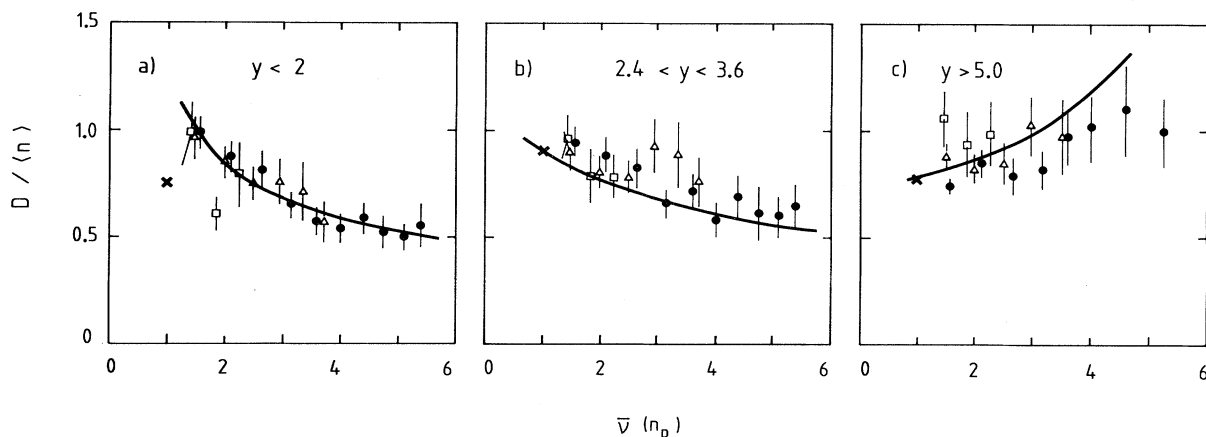


FIG. 9. Ratio  $D/\langle n \rangle$  of the distribution of the number of produced particles in (a) the target fragmentation, (b) the central production, and (c) the beam fragmentation regions versus  $\bar{\nu}(n_p)$ . Data for  $p\text{Xe}$ ,  $p\text{Ar}$ ,  $p\text{Ne}$ , and  $pp$  reactions are shown by circles, triangles, squares, and the cross, respectively. The solid curve in (a) is a fit of the form (6). Predictions of the AQM are shown by the solid curves in (b) and (c).

TABLE II. The average number  $\bar{\nu}(n_p)$  of projectile collisions and the average number  $\bar{\nu}_K$  of secondary collisions in the intranuclear cascade as a function of the number  $n_p$  of visible protons in 200-GeV/c  $p$ Ne,  $p$ Ar, and  $p$ Xe collisions.

$n_p$	Argon		$\bar{\nu}(n_p)$	Xenon		Neon	
	$\bar{\nu}(n_p)$	$\bar{\nu}_K$		$\bar{\nu}_K$	$\bar{\nu}(n_p)$	$\nu_K$	
0	1.52	0.3±0.2	1.54	-0.1±0.2	1.8	1.4±0.1	
1	2.03	2.0±0.2	2.10	2.2±0.3			
2	2.50	4.4±0.3	2.64	4.9±0.4			
3	2.94	6.3±0.5	3.14	7.7±0.5			
4	3.33	7.9±0.5	3.60	10.5±0.6			
5	3.68	9.7±0.6	4.02	14.5±0.8			
6			4.40	18.5±0.9			
7			4.75	21.7±1.1			
8			5.08	20.5±1.0			
9			5.38	26.0±1.1			

#### IV. ESTIMATE OF THE NUMBER OF COLLISIONS IN THE INTRANUCLEAR CASCADE

Whatever the nature of the object colliding with nucleons inside the nucleus, it brings either an extra positive charge when colliding with a proton, or no extra charge when colliding with a neutron. Thus one should observe an excess of positive charge, the value of which measures the total number of all collisions  $\nu_{\text{tot}}$  inside the nucleus.<sup>6</sup> Thus

$$\bar{\nu}_{\text{tot}} = \langle Q \rangle \frac{A}{Z}, \quad (7)$$

where  $\langle Q \rangle$  is the average net charge of all observed secondaries and  $A$  and  $Z$  are the mass and charge number of the nucleus. In this way  $\langle Q \rangle$  can be used to estimate the total number of collisions inside the nucleus independent of the number of knocked-out protons.

Knowing the total number  $\bar{\nu}_{\text{tot}}$  of collisions which have occurred inside the nucleus, and having estimated the number of projectile collisions  $\bar{\nu}(n_p)$  one can deduce how many collisions on average  $\bar{\nu}_K$  were due to secondary particles (i.e., cascading):

$$\bar{\nu}_K = \bar{\nu}_{\text{tot}} - \bar{\nu}(n_p). \quad (8)$$

Our results for  $\bar{\nu}_K$  for Ne, Ar, and Xe nuclei are given in Table II. The dependence of  $\bar{\nu}_K$  on  $\bar{\nu}(n_p)$  is shown in Fig. 10. From both Table II and Fig. 10 one sees that there is a strong correlation between these two numbers: the number of collisions of secondary particles increases rapidly with the number of projectile collisions, roughly as  $[\bar{\nu}(n_p)]^2$ . Moreover, this dependence is the same for different nuclei  $A$ . This may indicate that the formation zone of the cascading particles is larger than the differences between the radii of the studied nuclei.

#### V. CONCLUSIONS

We have studied 200-GeV/c  $pp$ ,  $p$ Ne,  $p$ Ar, and  $p$ Xe reactions in an experiment using a streamer-chamber spectrometer. Based on the hypothesis of independent consecutive collisions of a projectile inside the nucleus we have extracted the number of projectile collisions  $\bar{\nu}(n_p)$  from the data. Multiplicity and rapidity distributions were analyzed in terms of this parameter. We obtained the following results.

(i) The process of intranuclear cascading dominates in the target fragmentation region. It is characterized by a strong multiplication of particles, increasing linearly with  $\bar{\nu}(n_p)$  and by a ratio  $D/\langle n \rangle$  which decreases like  $1/[\bar{\nu}(n_p)]^{1/2}$ .

(ii) In the central rapidity region direct particle production from projectile collisions is expected to dominate. The particle multiplicity saturates at about three times the value observed in  $pp$  reactions. This indicates that the maximum number of effective projectile collisions is three.

(iii) In the beam fragmentation region the multiplicity falls below the value observed in  $pp$  collisions. This depletion is usually explained as a consequence of energy and momentum conservation.

(iv) The number of secondary collisions in the intranuclear cascade was estimated. It was found to increase like  $[\bar{\nu}(n_p)]^2$  for all nuclei.

The predictions of the additive quark model are in qualitative agreement with the results of this experiment.

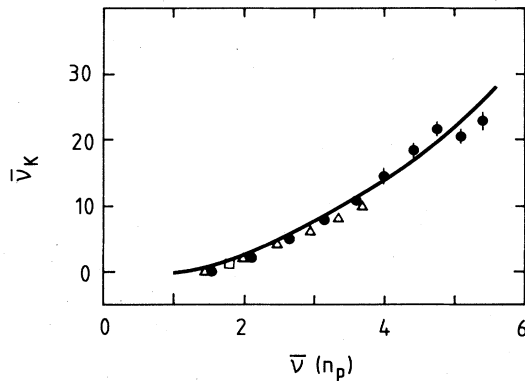


FIG. 10. Average number  $\bar{\nu}_K$  of secondary collisions in the intranuclear cascade versus the number  $\bar{\nu}(n_p)$  of projectile collisions for  $p$ Xe (circles),  $p$ Ar (triangles), and  $p$ Ne (squares) collisions. The curve of the form  $(\nu^{1.95} - 1)$  is shown for comparison.

## ACKNOWLEDGMENTS

It is a pleasure to acknowledge the excellent work of the engineers, the technicians, the programming and measuring teams at the collaborating institutions. We wish to thank the staff at CERN for the operation of the SPS ac-

celerator and the H2 beam line and for the contribution to the installation of the experiment. We have benefited from instructive discussions with A. Bialas. Liverpool would like to acknowledge the financial support of the SERC.

- <sup>1</sup>S. Brodsky, J. Gunion, and H. Kühn, *Phys. Rev. Lett.* **39**, 1120 (1977); Yu. M. Shabelski, *Yad. Fiz.* **26**, 1084 (1972) [*Sov. J. Nucl. Phys.* **26**, 577 (1977)]; A. Capella and A. Krzywicki, *Phys. Rev. D* **18**, 3357 (1978); A. Capella and J. Tran Thanh Van, *Phys. Lett.* **93B**, 146 (1980); W. Chao *et al.*, *Phys. Rev. Lett.* **44**, 518 (1980).
- <sup>2</sup>V. V. Anisovich, *Phys. Lett.* **B57**, 87 (1975); A. Bialas and W. Czyz, *Acta Phys. Pol.* **B10**, 831 (1979); V. V. Anisovich, Yu. M. Shabelski, and V. M. Shekter, *Nucl. Phys.* **B133**, 477 (1979); N. N. Nikolaev and A. Ya. Ostapchuck, CERN Report No. TH 2575, 1978 (unpublished); B. N. Levchenko and N. N. Nikolaev, MPI Report No. PAE-PTH 41/81 (unpublished).
- <sup>3</sup>A. Bialas and W. Czyz, *Phys. Lett.* **B51**, 179 (1974); A. Gurtu *et al.*, *Pramana* **3**, 311 (1974); W. Busza *et al.*, *Phys. Rev. Lett.* **34**, 836 (1975).
- <sup>4</sup>C. de Marzo *et al.*, *Phys. Rev. D* **26**, 1019 (1982).
- <sup>5</sup>B. Andersson, I. Otterlund, and E. Stenlund, *Phys. Lett.* **73B**, 343 (1978); M. K. Hegab and J. Hüfner, *Nucl. Phys.* **A384**, 353 (1982); N. Suzuki, *Prog. Theor. Phys.* **67**, 571 (1982); C. D. Rees *et al.*, *Z. Phys. C* **17**, 95 (1983).
- <sup>6</sup>F. Roesler and C. B. A. McCusker, *Nuovo Cimento* **10**, 127 (1953); I. Z. Artykov, V. S. Barashenkov, and S. M. Elisiev, *Nucl. Phys.* **B6**, 11 (1968); A. Dar and I. Vary, *Phys. Rev. D* **6**, 2412 (1972).
- <sup>7</sup>J. Babecki and G. Nowak, *Acta Phys. Pol.* **B9**, 401 (1978).
- <sup>8</sup>We used  $\bar{v}_A = 3.32$  (2.37) and  $\langle n_p \rangle_A = 3.92$  (1.91) in formula (2) for Xe (Ar).
- <sup>9</sup>W. Busza, *Acta Phys. Pol.* **B8**, 333 (1977).
- <sup>10</sup>A. Bialas and W. Czyz, *Phys. Lett.* **58B**, 325 (1975).
- <sup>11</sup>E. L. Feinberg and I. Pomeranchuk, *Nuovo Cimento Suppl.* **IV**, 652 (1956); W. N. Gribov, *Zh. Eksp. Teor. Fiz.* **56**, 892 (1969) [*Sov. Phys. JETP* **56**, 483 (1969)]; O. V. Kancheli, *Pis'ma Zh. Eksp. Teor. Fiz.* **18**, 469 (1973) [*JETP Lett.* **18**, 274 (1973)]; see also N. N. Nikolaev *et al.*, (Ref. 2).
- <sup>12</sup>A. Bialas and E. Bialas, *Phys. Rev. D* **20**, 2854 (1979).
- <sup>13</sup>A. Capella and J. Tran Thanh Van, in *Proton-Antiproton Collider Physics—1981*, proceedings of the Workshop, Madison, Wisconsin, edited by V. Barger, D. Cline, and F. Halzen (AIP, New York, 1982).
- <sup>14</sup>W. Busza, in *Proceedings of the Seventh International Colloquium on Multiparticle Production, Tutzing, Germany, 1976*, edited by J. Benecke *et al.* (Max Planck Institut, Munich, Germany, 1976), p. 545.